DOI: 10.1002/ejic.201001166

Influence of *N*-Substitution on the Oxidation of 2-Pyridylmethylamines with Bis(trimethylsilyl)amides of Iron(III) – Synthesis of Heteroleptic Iron(II) 2-Pyridylmethylamides

Astrid Malassa,[a] Benjamin Schulze,[a] Brigitte Stein-Schaller,[a] Helmar Görls,[a] Birgit Weber,[b] and Matthias Westerhausen*[a]

Keywords: Iron / Oxidation / Pyridylmethylamide ligands / Magnetic properties

The reaction of (thf)Fe[N(SiMe$_3$)$_2$]$_2$Cl with (2-pyridylmethyl)-(diphenylphosphanyl)amine (**1**) in hot tetrahydrofuran (THF) yields dinuclear [(ClFe)$_2${μ-N(SiMe$_3$)$_2$}{Ph$_2$P(NCH$_2$Py)$_2$}] (**2**) and [ClFe{Ph$_2$P(O)-NCH$_2$Py}]$_2$ (**3**) with the oxygen atom stemming from THF degradation. The formation of **2** requires a P–N bond cleavage and reformation leading to the tetradendate diphenyl-bis(2-pyridylmethylamido)phosphonium ion. If this reaction of (thf)Fe[N(SiMe$_3$)$_2$]$_2$Cl with **1** is performed at room temperature, no P–N bond cleavage is observed. Instead of that, ether degradation occurs yielding [Fe$_4$(μ$_4$-O)(μ$_2$-Cl)$_2$(Ph$_2$P-NCH$_2$Py)$_4$] (**4**) with a central oxygen-centered iron tetrahedron as well as complex **3**. Recrystallization of **3** from dichloromethane leads to addition of HCl and to the formation of [FeCl$_2$·{Ph$_2$P(O)-N(H)-CH$_2$Py}] (**5**). The phosphonium ion of **2** is isoelectronic to the corresponding diphenyl-bis(2-pyridylmethylamino)silane (**6**). Lithiation of **6** followed by a metathetical reaction with (thf)$_2$FeCl$_2$ yields the trinuclear complex [Fe$_3$Cl$_2${Ph$_2$Si(NCH$_2$Py)$_2$}$_2$] (**7**) with antiferromagnetic interactions.

Introduction

Picolylamines (2-pyridylmethylamines) and their deprotonated derivatives (picolylamides, 2-pyridylmethylamides) gained a tremendous importance in bioinorganic chemistry as models mostly for histidine in metal enzymes.[1] However, these ligands do not only behave as spectator ligands but are also involved in redox processes in the environment of transition metals. A general reactivity diagram is shown in Scheme 1 with protonation/deprotonation reactivity shown in the upper line and with oxidation/reduction equilibria presented in the column. The redox activity was often observed as an unexpected side reaction which is catalyzed by transition metal complexes such as, for example, cobalt(II) in the presence of air.[2] Iron complexes are well-known to oxidize hydrocarbons whereby the most reactive compounds often contain picolylamine fragments in the coordination spheres of the metal cations.[3–8]

Deprotonation of picolylamine (H_2L) yields the amides $(HL)^-$ which can be deprotonated again to $(L)^{2-}$ with strong bases such as Grignard reagents[9] or methyllithium in hexane.[10] These dianions $(L)^{2-}$ can be oxidized with e.g. white phosphorus[11] leading to the formation of $(L^{ox1})^-$. If the deprotonation reaction is performed with organometallics containing less electropositive metals, this oxidation process leads to precipitation of metal and immediately yields $(L^{ox1})^-$. This anion dimerizes and forms the tetradentate dianion $(L^{ox1}{}_2)^{2-}$. In the case of R being an alkyl group this equilibrium could be observed in solution whereas in the crystalline state only the dimer $(L^{ox1}{}_2)^{2-}$ was observed.[12] For R = SiR′$_3$ only the dimeric ligand $(L^{ox1}{}_2)^{2-}$ was found in solution and the solid state.[9,13] A second oxidation step leads to the formation of 2-pyridylmethylidene amines $(L^{ox2})^0$ which usually remain in the coordination sphere of the metals. This general reactivity depends not only on the oxidizing ability of the organometallics (redox potential of the metals) but also on the electronic nature and bulkiness of the *N*-bound substituent R.

The use of picolylamine (2-pyridylmethylamine, Py–CH_2–NH_2, R = H) offers not only the pathway shown in Scheme 1 but a second deprotonation step can also be performed at the amide functionality leading to imide Py–CH_2–N^{2-}. In addition with the lack of steric protection a variety of subsequent reactions are possible leading to numerous products. Thus, the reaction of methylzinc picolylamide with dimethylzinc leads to C–C coupling reactions but these intermediate products $(MeZn)_2(L^{ox1}{}_2)$ (R = H) show a similar reactivity than the starting materials and undergo subsequent degradation reactions.[14] Substitution

[a] Institut für Anorganische und Analytische Chemie, Friedrich-Schiller-Universität Jena,
August-Bebel-Str. 2, 07743 Jena, Germany
Fax: +49-3641-948102
E-mail: m.we@uni-jena.de
[b] Anorganische Chemie II, Universität Bayreuth,
Universitätsstraße 30, NW I, 95440 Bayreuth, Germany
Fax: +49-921 552157
E-mail: weber@uni-bayreuth.de
Supporting information for this article is available on the WWW under http://dx.doi.org/10.1002/ejic.201001166.

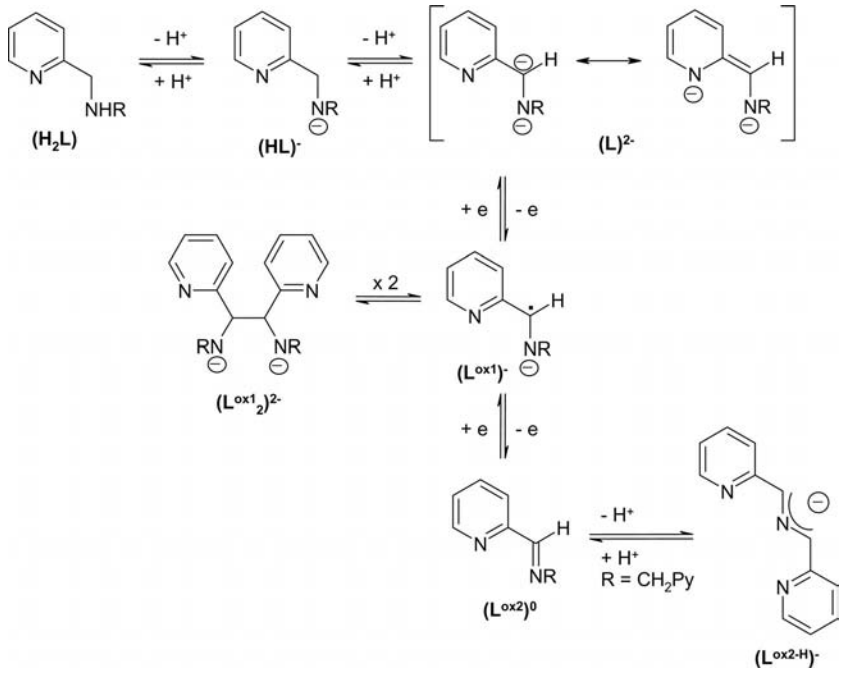

Scheme 1. Reactivity diagram of picolylamine. The upper row shows the deprotonation/protonation equilibria, the column outlines the redox equilibria.

of this hydrogen atom by a *N*-bound trialkylsilyl group hinders these degradation reactions and $(L^{ox1}_2)^{2-}$ is accessible with good yields.[9,13] Bulky aryl substituents such as 2,6-diisopropylphenyl groups at the amido unit stabilize the radical anion $(L^{ox1})^-$ and allow the crystallization of homoleptic compounds $[M(L^{ox1})_2]$ (M = Cr, Mn, Fe, Co, Ni, Zn).[15]

A second oxidation of the radical anion $(L^{ox1})^-$ leads to the formation of neutral 2-pyridylmethylidene amines $(L^{ox2})^0$. Even though iron(II) and iron(III) complexes of picolylamine (H_2L) are stable,[16,17] complexes containing amides $(HL)^-$ are strongly destabilized due to the fact that these anions represent strong σ- and strong π-donors which disfavour complexes with electron-rich late transition metals.[18] Therefore, the doubly deprotonated species $(L)^{2-}$ are unstable in the presence of strong oxidizing reagents such as, for example, cobalt(III)[19] and iron(III)[20] leading immediately to the imines $(L^{ox2})^0$. These imines are bound at the metal(II) cations or readily form adducts with iron(II) complexes.[21]

More complicated situations can be expected for dipicolylamines [bis(2-pyridylmethyl)amines] because two methylene moieties are now available for a second metalation reaction. Again, iron(II) complexes of dipicolylamine are stable with this ligand acting as a tridentate chelate ligand coordinating in a facial manner.[17,22,23] In contrast to cobalt(II) chloride, the iron(II) chloride complexes react differently with air: Oxygen inserts between the iron atoms raising the oxidation state from iron(II) to iron(III) without oxidation of the coordinated bis(2-pyridylmethyl)amine molecules.[22]

As expected from the findings described above, deprotonation of dipicolylamine leads to very reactive iron(II) bis(dipicolylamide) which precipitates from the reaction mixture thus preventing subsequent degradation reactions.[23,24] However, soluble heteroleptic RM-N$(CH_2$-Py$)_2$ (M = Mn, Fe, Co, Zn) as well as the metallation of dipicolylamine with $M[N(SiMe_3)_2]_2$ lead to the formation of metal(II) bis[1,3-bis(2-pyridyl)-2-azapropenide] $(L^{ox2-H})^-$ (see Scheme 1).[23,25] These complexes are stable and also accessible via metalation of *N*-picolyl-(2-pyridylmethylidene)amine or metathetical via the reaction of lithium [1,3-bis(2-pyridyl)-2-azapropenide] with metal halides.[24] A similar reaction sequence for dipicolylamine can be assumed because intermediate structures of the type $(HL)^-$ (dipicolylamide) and $(L^{ox2})^0$ [*N*-picolyl(2-pyridylmethylidene)-amine] were found in the vicinity of rhodium(I)[26] and iridium(I) starting from metalated dipicolylamine.[27]

In order to further elucidate the influence of the *N*-bound substituent, we investigated the reaction of iron-based metalation reagents with *N*-diphenylphosphanyl-picolylamine[28] which offers an additional Lewis base.

Results and Discussion

In order to estimate the electronic stabilization of 2-pyridylmethylamines by N-bound substituents, (2-pyridylmethyl)(diphenylphosphanyl)amine (**1**)[27] was included in our investigations. Depending on the reaction conditions two different products were isolated from the reaction of (thf)Fe$[N(SiMe_3)_2]_2$Cl with **1** in THF solutions. In hot THF, the pale yellow dinuclear complex **2** was isolated after eight hours according to equation (1). Whereas **2** precipitated as single crystalline material, complex **3** precipitated as a microcrystalline powder. In complex **2**, a new tetradentate ligand was formed which can be regarded as a phos-

phonium cation with two phenyl and two 2-pyridylmethylamido groups. During this reaction, a reduction of iron(III) to iron(II) was observed. One of the bis(trimethylsilyl)amido ligands was maintained as a bridging ligand in the coordination spheres of the metal atoms which is not unusual; e.g. in dimeric $[Fe\{N(SiMe_3)_2\}_2]_2$ also bridging $N(SiMe_3)_2$ groups exist (Fe–N_{term} 192.5 pm, Fe–N_{br} 208.5 pm).[29] As observed earlier, the iron-bound chlorine atoms showed no reactivity towards this secondary amine and were preserved at iron; see Equation (1).

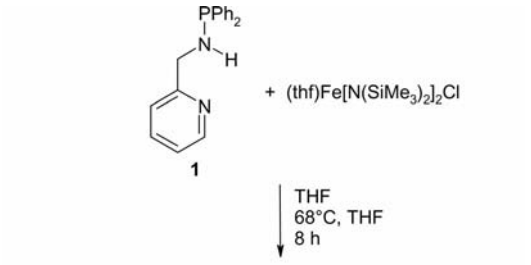

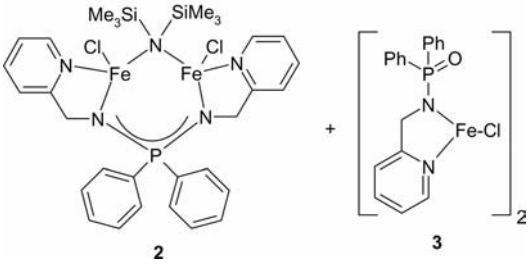

(1)

At room temperature a very slow reaction was observed and within two weeks bright red crystals of tetranuclear **4** precipitated besides already known complex **3**; see Equation (2). In **4**, the iron atoms form an oxygen-centered Fe_4 tetrahedron. Two opposite Fe···Fe edges are bridged by chlorine atoms. In addition each iron(II) atom is bound to the nitrogen atoms of the bidentate (2-pyridylmethyl)(diphenylphosphanyl)amido substituent whereas the diphenylphosphanyl moiety coordinates to another iron center. Thus, all iron atoms exhibit a coordination number of five (two N, O, Cl, P). Such a tetrahedral $(Fe_4O)^{6+}$ unit was observed earlier by, for example, Cotton et al.,[30,31] The oxygen source was most probably the THF solvent which was oxidized and cleaved by iron(III). Similar to the *N*-trialkylsilyl-substituted 2-pyridylmethylamides, no complexes of iron(III) with (2-pyridylmethyl)(diphenylphosphanyl)amides were observed.

We were unable to obtain single crystals of **3** but the composition of this compound was deduced from analytical data. In order to prove the constitution of this iron(II) complex (2-pyridylmethyl)(diphenylphosphanyl)amine (**1**) was lithiated and then reacted with $FeCl_3$ in THF solution. During this redox reaction the phosphorus atom was oxidized and the resulting complex **3** showed the same analytical data as the microcrystalline material shown in Equation (1) and (2). Recrystallization of **3** from dichloromethane led to the addition of HCl and finally yielded an adduct of

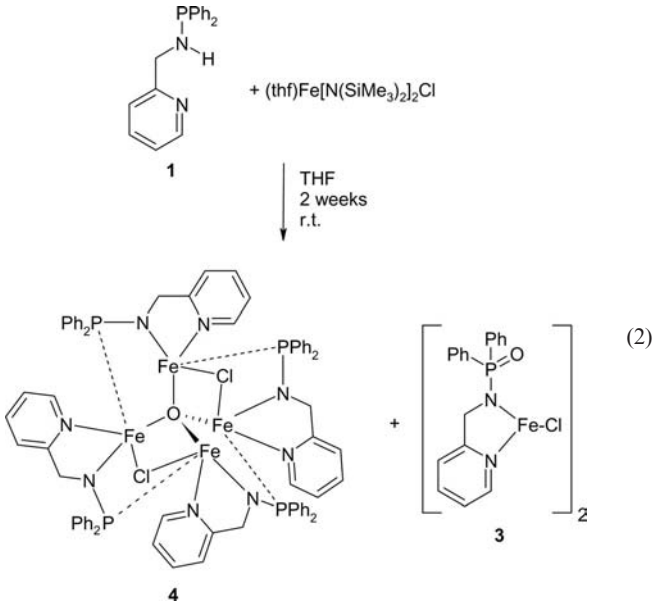

(2)

picolylamino-diphenylphosphane oxide at iron(II) chloride (**5**) according to Equation (3). An X-ray diffraction experiment verified that ligand **3** binds via the oxygen atom to the iron(II) cation.

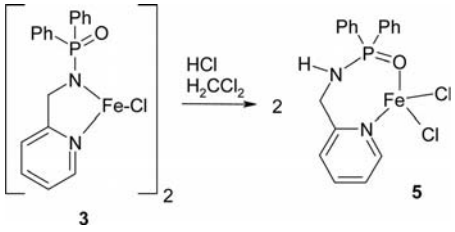

(3)

None of the above mentioned reactions allowed the oxidative C–C bond formation to yield $(L^{ox1}{}_2)^{2-}$ or the isolation of an iron complex of the imine $(L^{ox2})^0$ (see Scheme 1). Instead of the synthesis of these oxidized ligands P–N bond cleavage and THF degradation was observed because the oxygen atoms in compounds **3** and **4** stem from ether cleavage reactions; hydrolysis (reaction with water) and oxidation with oxygen (air) can safely be excluded. On the one hand, iron(III) chloride hexa(hydrate) proofed to be an unsuitable starting material for the reaction with (2-pyridylmethyl)(diphenylphosphanyl)amine (**1**). Also the presence of oxygen did not enhance the yield of $[\{(Ph_2PN\text{-}CH_2\text{-}2\text{-}Py)Fe\}_4(\mu\text{-}Cl)_2(\mu_4\text{-}O)]$ (**4**). On the other hand, ether cleavage reactions are well-known side reactions in the chemistry of electropositive metals,[32,33] but also in iron-based chemistry.[34–37] Li and co-workers[34] described in detail the degradation of THF in the vicinity of iron(III); addition of TEMPO suppressed this THF degradation. This finding was interpreted in the sense of a radical mechanism.

The substitution of the P^+ atom of the tetradentate ligand of **2** by a silicon atom yields an isoelectronic tetradentate ligand. In order to investigate the coordination behav-

iour of this ligand, we reacted $[PyCH_2N(H)]_2SiPh_2$ (**6**) with two equivalents of *n*BuLi and thereafter with an appropriate amount of $(thf)_2FeCl_2$ according to Equation (4). The trinuclear complex **7** combines two well-known structural units, namely the heteroleptic dimeric 2-pyridylmethylamido iron(II) chloride moiety and the iron(II) bis(2-pyridylmethylamide) unit which are interconnected via diphenylsilyl fragments.

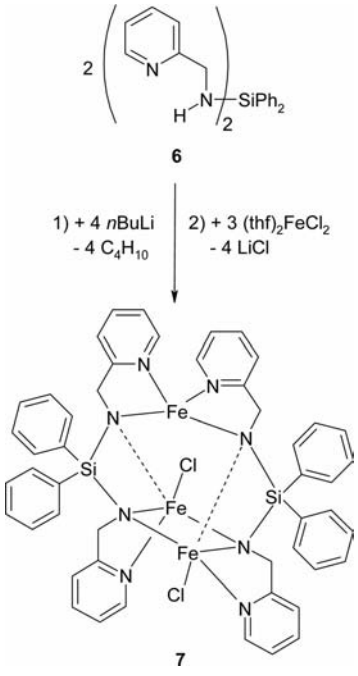

(4)

Molecular Structures

Molecular structure and numbering scheme of **2** are represented in Figure 1. The iron atoms are in distorted tetrahedral environments. Due to the electrostatic attraction the Fe1–N2 and Fe2–N3 bond lengths of the amide are with an average value of 202.4 pm significantly shorter than the Fe–N distances to the pyridyl units with an average value of 214.1 pm.

The phosphonium ligand shows average P–C and P–N bond lengths of 181.8 and 160.6 pm, respectively. Comparable bis(benzylamido)diphenylphosphonium anions show similar P–N bond lengths between 160 and 163 pm and act as bidentate ligands at titanium and zirconium.[38] The deviation of the angles at P1 in **3** from tetrahedral geometry is smaller than ±4°. The N–P–N values between 95 and 98° for the group 4 complexes with bis(benzylamido)diphenylphosphonium ligands are much smaller. The coordination behaviour of the tetradentate bis(2-pyridylmethylamido)diphenylphosphonium anions in **3** deviates significantly because the iron atoms are bound to the 2-pyridylmethylamido moieties forming five-membered rings whereas the bis(benzylamido)diphenylphosphonium unit is only able to behave as a bidentate ligand via the amido nitrogen bases.

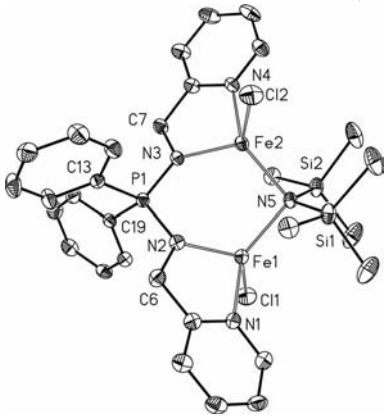

Figure 1. Molecular structure and numbering scheme of $[(ClFe)_2\{Ph_2P(N\text{-}CH_2\text{-}2\text{-}Py)_2\}\{\mu\text{-}N(SiMe_3)_2\}]$ (**2**). The ellipsoids represent a probability of 40%, H atoms are neglected for clarity reasons. Selected bond lengths [pm]: Fe1–N1 213.8(3), Fe1–N2 202.5(3), Fe1–N5 209.1(3), Fe1–Cl1 227.9(1), Fe2–N3 202.2(3), Fe2–N4 214.4(3), Fe2–N5 209.9(3), Fe2–Cl2 226.4(1), P1–N2 160.8(3), P1–N3 160.3(3), P1–C13 181.7(4), P1–C25 186.9(4), N2–C6 146.8(4), N3–C7 146.0(4), N5–Si1 177.0(2), N5-Si2 176.2(3); angles [°]: Cl1–Fe1–N1 95.14(8), Cl1–Fe1–N2 122.42(8), Cl1–Fe1–N5 117.87(8), N1–Fe1–N2 78.9(1), N1–Fe1–N5 125.9(1), N2–Fe1–N5 110.9(1), Cl2–Fe2–N3 121.68(8), Cl2–Fe2–N4 95.39(8), Cl2–Fe2–N5 117.12(7), N3–Fe2–N4 79.0(1), N3–Fe2–N5 112.1(1), N4–Fe2–N5 125.9(1), Si1–N5–Si2 119.3(2).

The bridging bis(trimethylsilyl)amido ligand displays rather large Si–N5 bond lengths of 176.6 pm due to the coordination number of four and sp^3 hybridization for N5. The Si1–N5–Si2 angle of 119.3(2)° is the largest angle at N5 due to the repulsion of the bulky trimethylsilyl groups. The rather large Fe–N bond lengths allow a small angle of 99.5(1)° whereas the Fe–N5–Si angles adopt values between 106.4(1) and 111.7(1)°. Due to the steric strain induced by the bulky $SiMe_3$ groups the Fe–N5 distances with an average value of 209.5 pm are larger than the Fe1–N2 and F2–N3 bond lengths.

The molecular structure of $[Fe_4\{N(PPh_2)CH_2Py\}_4Cl_2O]$ (**4**) is displayed in Figure 2. Symmetry-related atoms are marked with the letters "A" ($-y + 5/4$, $x - 3/4$, $-z + 5/4$), "B" ($y + 3/4$, $-x + 5/4$, $-z + 5/4$), and "C" ($-x + 2$, $-y + 1/2$, z). The central structural fragment consists of an oxygen-centered iron(II) tetrahedron. Two opposite Fe···Fe edges are bridged by chlorine ligands, all other edges are bridged by the N–P bonds of the (2-pyridylmethyl)(diphenylphosphanyl)amido substituents. All iron(II) atoms are embedded in a trigonal bipyramidal environment with the oxygen atom and the pyridyl group in apical positions [O–Fe–N1 175.03(8)°]. The equatorial positions are occupied by Cl, P, and N2 atoms. Distortions from the trigonal bipyramidal coordination sphere result from the bite of the 2-pyridylmethylamido unit leading to a N1–Fe–N2 angle of only 76.3(1)°.

In **5** a Fe–O distance of 202.87(5) pm is observed (Figure 3). This value is in agreement to the Fe–O distances of the discrete $[Fe_4(\mu\text{-}O)]^{6+}$ unit with an average value of 198.3 pm (varying between 193.4(5) and 201.0(5) pm) reported by Cotton and co-workers[30] for $[Fe_4(NPy_2)_6O]$; the

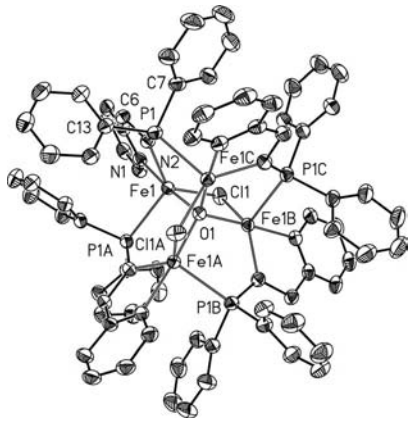

Figure 2. Molecular structure and numbering scheme of [{(Ph_2PN-CH_2-2-Py)Fe}$_4$(μ-Cl)$_2$(μ_4-O)] (**4**). Ellipsoids represent a probability of 40%, H atoms are omitted for clarity reasons. Symmetry-related atoms are labelled with the letters "A" ($-y$ + 5/4, x – 3/4, $-z$ + 5/4), "B" (y + 3/4, $-x$ + 5/4, $-z$ + 5/4), and "C" ($-x$ + 2, $-y$ + 1, z). Hydrogen atoms are not shown. Selected bond lengths [pm]: Fe1–O1 202.87(5), Fe1–Cl1 250.1(1), Fe1–P1 246.8(1), Fe1–N1 223.1(3), Fe1–N2 201.0(3), P1–N2 164.9(3), P1–C7 183.3(4), P1–C13 184.0(4), N2–C6 146.1(5); angles [°]: Fe1–O1–Fe1A 112.92(2), Fe1–O1–Fe1B 112.93(2), Fe1–O1–Fe1C 102.77(3), O1–Fe1–Cl1 89.28(3), O1–Fe1–N1 175.03(8), O1–Fe1–N2 103.75(9), O1–Fe1–P1A 95.30(3).

slightly smaller value stems from the smaller coordination number of four for one of the iron(II) atoms. Due to a strong electrostatic attraction between the positive metal center and the negatively charged amido function a short Fe–N2 bond of 201.0(3) was found whereas in [Fe_4(NPy_2)$_6$O] of Cotton et al.[30] the negative charge is delocalized within the whole ligand, leading to a reduced electrostatic attraction and larger Fe–N distances. The Fe–Cl bond lengths of 250.1(1) pm are significantly larger (approx. 10%) than observed for the terminal Cl substituents in **2** (Table 1). This fact can be addressed to the bridging positions of the chloride anions and to the larger coordination number of the iron atoms.

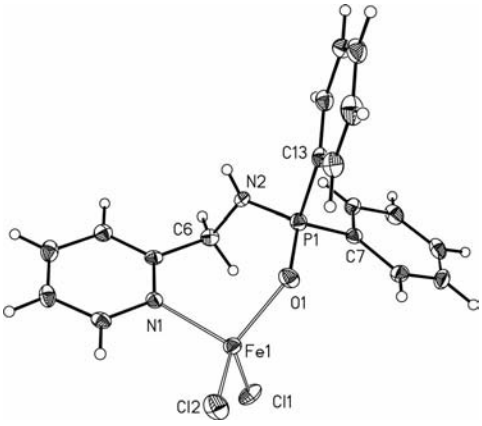

Figure 3. Molecular structure and numbering scheme of [{2-Py-CH_2-N(H)-P(O)Ph_2}$FeCl_2$] (**5**). Selected bond lengths [pm]: Fe1–O1 198.3(2), Fe1–N1 213.8(3), Fe1–Cl1 228.52(9), Fe1–Cl2 226.20(9), P1–O1 150.6(2), P1–N2 161.9(3), P1–C7 178.9(3), P1–C13 179.3(3), N2–C6 146.8(4), C5–C6 150.8(4); angles [°]: O1–Fe1–N1 102.74(9), O1–Fe1–Cl1 116.54(7), O1–Fe1–Cl2 108.96(6), N1–Fe1–Cl1 97.66(7), N1–Fe1–Cl2 112.93(7), Cl1–Fe1–Cl2 116.67(4), O1–P1–N2 115.7(1), P1–N2–C6 123.1(2), N2–C6–C5 111.9(2).

Table 1. Crystal data and refinement details for the X-ray structure determinations of the compounds **2**, **4**, **5**, 6 and **7**.

Compound	**2**	**4**	**5**	**6**	**7**
Formula	$C_{30}H_{40}Cl_2Fe2N_5PSi_2$·$C_4H_8O$	$C_{72}H_{64}Cl_2F_4$ N_8OP_4·4(C_4H_8O)	$C_{18}H_{17}Cl_2FeNOP$	$C_{24}H_{24}N_4Si$	$C_{48}H_{44}Cl_2Fe_3N_8Si_2$·1.25$C_4H_8O$
Fw [g mol^{-1}]	812.52	1763.91	435.06	396.56	1117.67
T [°C]	–90(2)	–90(2)	–90(2)	–90(2)	–90(2)
Crystal system	triclinic	tetragonal	monoclinic	monoclinic	monoclinic
Space group	$P\bar{1}$	$I4_1/a$	$P2_1/n$	$P2_1/c$	$C2/c$
A [Å]	11.4040(5)	17.2104(4)	12.9227(7)	10.9830(3)	29.0168(6)
B [Å]	13.0271(6)	17.2104(4)	11.6608(6)	8.7586(4)	14.3573(2)
c [Å]	14.3238(5)	34.3545(8)	13.7635(7)	22.0613(8)	29.3947(7)
A [°]	100.878(3)	90	90	90	90
B [°]	105.210(2)	90	113.760(3)	100.611(3)	110.805(1)
γ [°]	100.136(2)	90	90	90	90
V [Å^3]	1958.60(14)	10175.7(4)	1898.22(18)	2085.91(13)	11447.4(4)
Z	2	4	4	4	8
ρ [g cm^{-3}]	1.378	1.151	1.522	1.263	1.297
μ [mm^{-1}]	10.13	7.21	11.69	1.3	9.29
Measured data	13406	34376	12552	13892	30551
Data with $I>2\sigma(I)$	5344	4177	2737	3147	8336
Unique data (R_{int})	8860/0.0392	5822/0.0533	4326/0.0746	4759/0.0538	12827/0.0564
wR_2 (all data, on F_2)[a]	0.1277	0.2307	0.1047	0.1218	0.2223
R_1 [$I>2\sigma(I)$][a]	0.0511	0.0665	0.0443	0.0468	0.0734
S[b]	1.006	1.031	0.998	1.006	1.021
Residual electron density [e Å^{-3}]	0.424/–0.420	0.839/–0.458	0.175/–0.187	0.257/–0.344	0.296/–0.349
Absorption method	none				

[a] Definition of the R indices: $R_1 = (\Sigma||F_o| - |F_c||)/\Sigma|F_o|$. $wR_2 = \{\Sigma[w(F_o^2 - F_c^2)^2]/\Sigma[w(F_o^2)^2]\}^{1/2}$ with $w^{-1} = \sigma^2(F_o^2) + (aP)^2 + bP$; $P = [2F_c^2 + \max(F_o^2)/3]$. [b] $s = \{\Sigma[w(F_o^2 - F_c^2)^2]/(N_o - N_p)\}^{1/2}$.

Due to reduced electrostatic attraction in comparison to complex **4**, the P–C (average 183.7 pm) and P–N2 bonds [164.9(3) pm] are elongated. In **4** the tetradentate bis(2-pyridylmethylamido)diphenylphosphonium ligand contains a positively charged P atom which has a smaller radius than a neutral P atom in **5** with a phosphanyl group. The N2 atom displays a nearly planar coordination sphere (angle sum at N2 359.4°).

The molecular structure of **6** is represented in Figure 4. The Si–N bonds with an average value of 170.5 pm are rather short. The planar coordination spheres of N1 and N3 suggest an sp^2(N) hybridization with the possibility of the p_z(N) lone pair to interact with σ*(Si–C) bonds. The Si–C bond lengths display an average value of 186.7 pm. The coordination sphere of the silicon atom shows only slight deviations from the tetrahedron.

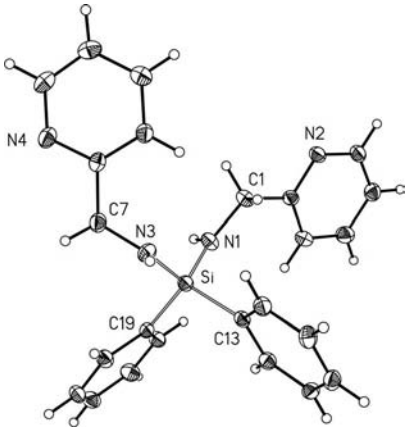

Figure 4. Molecular structure and numbering scheme of [$Ph_2Si(NH\text{-}CH_2\text{-}2\text{-}Py)_2$] (**6**). The ellipsoids represent a probability of 40%. Selected bond lengths [pm]: Si–N1 170.8(2), Si–N3 170.2(2), Si–C13 186.8(2), Si–C19 186.5(2), N1–C1 145.5(2), N3–C7 145.3(2); angles [°]: N1–Si–N3 113.59(9), N1–Si–C13 110.03(8), N1–Si–C19 104.59(9), N3–Si–C13 106.37(9), N3–Si–C19 111.54(8), C13–Si–C19 110.80(8), Si–N1–C1 124.2(2), Si–N3–C7 122.5(2), N1–C1–C2 115.0(2), N3–C7–C8 115.1(2).

Figure 5 shows the molecular structure of **7**. The bis(2-pyridylmethylamido)diphenylsilane ligands are distinguished by the letters "A" and "B". The iron atom Fe1 is in a distorted tetrahedral environment whereas the pentacoordinate Fe2 and Fe3 atoms display distorted trigonal bipyramidal coordination spheres. The Cl1–Fe2–N3A and Cl2–Fe3–N3B angles show values of 151.7(1)° and 152.6(1)°, respectively. Due to the coordination number of five for Fe2 and Fe3, an elongation of the Fe–Cl bonds (average 237.2 pm) is observed in comparison to **2**. For the same reason, the Fe1–N distances are significantly smaller than the Fe2–N and Fe3–N values of the pentacoordinate iron(II) atoms. The environment of Fe1 is comparable to $Fe[N(SiMe_2tBu)CH_2Py]_2$,[21] however, in **3** the N–Fe–N angle of the amido functions was widened [155.5(1)°] due to the bulky *tert*-butyldimethylsilyl groups. In **7** the N2A–Fe1–N2B bond angle displays a value of 125.7(2)° due to a reduced steric hindrance at the silyl fragments.

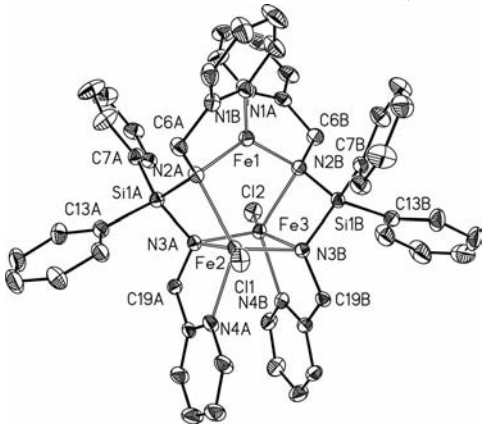

Figure 5. Molecular structure and numbering scheme of [$Cl_2Fe_3\{Ph_2Si(N\text{-}CH_2\text{-}2\text{-}Py)_2\}_2$] (**7**). Ellipsoids represent a probability of 40%, H atoms are omitted for clarity reasons. The ligands are distinguished by the letters "A" and "B". Selected bond lengths [pm]: Fe1–N1A 208.5(4), Fe1–N2A 199.8(4), Fe1–N1B 209.3(5), Fe1–N2B 199.6(4), Fe2–Cl1 236.6(1), Fe2–N2A 224.1(4), Fe2–N3A 221.6(4), Fe2–N4A 217.9(4), Fe2–N3B 205.3(4), Fe3–Cl2 237.8(1), Fe3–N2B 219.7(4), Fe3–N3B 223.0(4), Fe3–N4B 216.9(4), Fe3–N3A 206.0(4), Si1A–N2A 172.7(4), Si1A–N3A 172.0(4), Si1B–N2B 173.0(4), Si1B–N3B 171.1(4), N2A–C6A 147.1(6), N3A–C19.A 146.3(6), N2B–C6B 146.4(6), N3B–C19B 147.6(6).

The iron atom Fe2 binds to the three nitrogen atoms N2A, N3A, and N4A of the ligand A, Fe3 to N2B, N3B, and N4B of ligand B. This fact leads to small N2–Si1–N3 bond angles of 98.2(2)° (ligand A) and 99.2(2)° (ligand B) whereas free $Ph_2Si[N(H)CH_2Py]_2$ (**6**) shows an N–Si–N angle of 113.59(9)°. The tetracoordinate amido N atoms N2 and N3 show a distorted tetrahedral coordination sphere which reduces the possibility of hyperconjugation [back-donation of charge from p_z(N) into σ*(Si–C)] thus leading to an elongation of the Si–N bonds (average Si–N 172.2 pm).

Magnetic Properties

Whereas the magnetic properties of **2** and **4** were discussed earlier[39] the iron atoms in complex **7** show an arrangement as an isosceles triangle. Magnetic susceptibility measurements were performed in the temperature range from 300 K to 2 K for the trinuclear complex **7** using a Quantum design MPMSR-5S-SQUID magnetometer. Figure 6 displays the thermal dependence of the $\chi_M T$ product (with χ_M being the molar susceptibility and T the temperature) at 0.2 T. The room temperature value is with 5.32 $cm^3\,K\,mol^{-1}$ significantly lower than the expected one for three non-interacting $S = 2$ centers (9.00 $cm^3\,K\,mol^{-1}$ for $g = 2$). Upon cooling the $\chi_M T$ product decreases further to reach a plateau at 60 K with an average value of $\chi_M T$ = 3.58 $cm^3\,K\,mol^{-1}$. This value is in the region expected for one iron(II) center with considerable orbital momentum. Below 25 K the $\chi_M T$ product decreases further, most likely this can be attributed to zero-field splitting. The observed behaviour is typical for trinuclear systems with antiferromagnetic interactions.

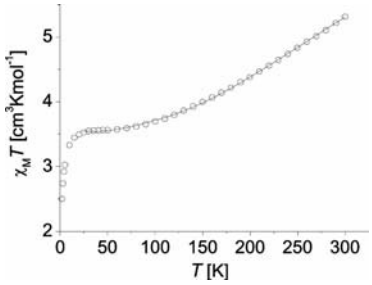

Figure 6. Plot of the $\chi_M T$ product (open circles) vs. T for compound **7** at 0.2 T. The solid line represents the calculated temperature dependence with the model described in the text.

The results from the X-ray structure analysis indicate that the system is best described as isosceles triangle ABA with J and J' as interaction parameters. Fe2 and Fe3 (A and A′) are linked over two bridging nitrogen atoms (N3A and N3B) with a Fe2···Fe3 distance of 281.79(9) pm and a Fe–N–Fe angle of 82.4°. The Fe1–Fe2 (and Fe1–Fe3 with Fe1 = B) interaction is mediated over the bridging nitrogen atom N2A (N2B) with Fe1···Fe2 and Fe1···Fe3 distances of 321.6(2) and 306.7(2) pm, respectively, and a Fe–N–Fe bond angle of 98.5°. For such trinuclear systems with antiferromagnetic interactions it is not possible to align all local spins antiparallel to each other as illustrated in Figure 7. Therefore, the ratio $\rho = J'/J$ (with J being the A–B interaction parameter and J' corresponding to the A–A interaction parameter) is of interest in order to distinguish between the possible interaction schemes given in Figure 7.

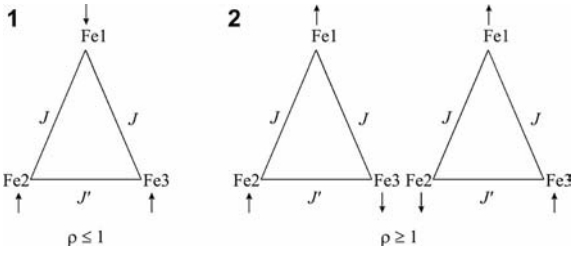

Figure 7. Schematic representation of the possible interaction schemes in an isosceles triangle in dependence of the ratio $\rho = J'/J$.

For the determination of J and J' the data were analysed assuming three interacting S = 2 spin centres with the Hamiltonian given as[40]

$$H = -J(S_{A1}S_B + S_{A2}S_B) - J'S_{A1}S_{A2}$$

where the local spins are denoted S_{A1}, S_{A2} and S_B. The resulting expression for the magnetic susceptibility is given in the Supporting Information. A good agreement between calculated and experimental data was obtained with the parameters $J = -55.6 \pm 1.9$ cm^{-1}, $J' = 6.0 \pm 0.4$ cm^{-1}, $g_A = 3.12 \pm 0.03$, and $g_B = 3.20 \pm 0.06$. The strong A–B antiferromagnetic interaction polarizes S_{A1} and S_{A2} ferromagnetically (case 1 in Figure 7). As each iron center has four unpaired electrons the determination of the exact interaction path between the iron centers is difficult.

Conclusions

Amides are strong σ- and π-donors and hence, reactive metal-nitrogen bonds are formed with electron-rich late 3d metals. 2-Pyridylmethylamides offer a variety of possible reaction pathways such as deprotonation of the methylene unit together with redox behaviour (see Scheme 1) finally leading to 2-pyridylmethylidene amines (2-pyridylmethylimines). *N*-Bound trialkylsilyl groups support this reaction Scheme and mainly the redox potential of the metal atom determines whether a dianion $(L)^{2-}$ (lithium, magnesium), a radical $(L^{ox1})^-$ or its dimer $(L^{ox1}{}_2)^{2-}$ (zinc), or even an electroneutral imine $(L^{ox2})^0$ [iron(III)] is formed. Substitution of the silyl group by a diphenylphosphanyl moiety (**1**) expands the reactivity pattern in the presence of iron(III). In THF solution cleavage of P–N bonds and formation of bis(2-pyridylmethylamido) diphenylphosphonium anions (bound at Fe^{II} as in **2**) are observed. This reaction is accompanied by oxidative THF degradation reactions leading to oxygen-centered iron cages (with Fe_4O fragments as in **4**) and to (2-pyridylmethylamido) diphenylphosphane oxide anions (bound at Fe^{II} as in **3**). Addition of HCl to **3** yields neutral (2-pyridylmethylamino)diphenylphosphane oxide in the vicinity of iron(II) (as a $FeCl_2$ adduct as in **5**). We were unable to isolate C–C coupled amides of the type $(L^{ox1}{}_2)^{2-}$ or imines such as $(L^{ox2})^0$. The silicon-based ligand isoelectronic to the bis(2-pyridylmethylamido) diphenylphosphonium anion, namely bis(2-pyridylmethylamido) diphenylsilane (**6**), expresses a straight-forward coordination behaviour and trinuclear **7** was obtained. Each iron center in this trinuclear complex has four unpaired electrons. The antiferromagnetic coupling between two of these iron(II) atoms (high spin $3d^6$ iron cations) leads to a spin-frustrated system.

Experimental Section

General: All manipulations were carried out in an argon atmosphere under anaerobic conditions. Prior to use, all solvents were thoroughly dried and distilled in an argon atmosphere. The reported iron complexes are moisture and air sensitive. DEI-mass spectra were obtained on a Finnigan MAT SSQ 710 system (2,4-dimethoxybenzyl alcohol as matrix), IR measurements were carried out on a Perkin–Elmer System 2000 FT-IR. Starting [(thf)-Fe{N(SiMe$_3$)$_2$}$_2$Cl],[36,41] Py-CH$_2$-N(H)-PPh$_2$ (**1**),[28] and Py-C(Ph)-H-N(H)-PPh$_2$[42] were prepared according to literature procedures.

(ClFe)$_2${Ph$_2$P(*N*-CH$_2$-2-Py)$_2$}{μ-*N*(SiMe$_3$)$_2$} (2): A solution of 0.33 g of Py-CH$_2$-N(H)-PPh$_2$ (**1**) (1.12 mmol) in 10 mL of THF was added at room temp. to a solution of 0.59 g of [(thf)-Fe{N(SiMe$_3$)$_2$}$_2$Cl] (1.22 mmol). This reaction mixture was heated under reflux for 6 h. After cooling to room temp. the volume of the solution was reduced until crystal formation was observed. At room temp. 0.11 g of pale yellow crystals of **2** (0.15 mmol, 25%) precipitated which were washed with a few mL of THF and dried in vacuo. Prolonged crystallization for several days at room temp. also afforded crystals of [{2-Py-CH$_2$-N-P(O)Ph$_2$}FeCl] (**3**).

Physical Data of 2: M.p. 175 °C. IR (Nujol, KBr windows): $\tilde{\nu}$ = 1606 (m), 1569 (w), 1483 (m), 1437 (m), 1287 (m), 1246 (m), 1145 (s), 1112 (m), 1065 (w), 1050 (w), 1019 (w), 943 (m), 871 (s), 846

(m br), 757 (m), 720 (m), 699 (m), 674 (w), 650 (w), 599 (w), 567 (m), 537 (m), 512 (m), 488 (w). MS (DE): *m*/*z* (%) = 488 (10) [{(Py-$CH_2N)_2PPh_2$}FeCl]$^+$, 452 (5) [{(Py-$CH_2N)_2PPh_2$}Fe]$^+$, 161 (50) [$HN(SiMe_3)_2$]$^+$, 146 (97) [$HNSi_2Me_5$]$^+$, 130 (100) [$HNSi_2Me_4$]$^+$. $C_{34}H_{48}Cl_2Fe_2N_5OPSi_2$ (812.52): calcd. C 50.26, H 5.95, N 8.62; found C 49.88, H . 5.78, N 8.96.

[{(Ph_2PN-CH_2-2-Py)Fe}$_4$(μ-Cl)$_2$(μ$_4$-*O*)] (4): A solution of 0.38 g of Py-CH_2-N(H)-PPh_2 (**1**) (1.30 mmol) in 10 mL of THF was dropped at room temp. into a solution of 0.62 g of [(thf)Fe{$N(SiMe_3)_2$}$_2$Cl] (1.30 mmol). Thereafter, stirring was continued for 43 h. Then the volume of the solution was reduced to 5 mL in vacuo. This solution was stored at room temp. and after a few days, dark red, octahedron-shaped crystals of **4** precipitated. After collection of these crystals the mother liquor was stored at room temp. and colorless needles of [{2-Py-CH_2-N-P(O)Ph_2}FeCl] (**3**) formed. Yield of single-crystalline **4**: 0.08 g (0.06 mmol, 18%); m.p. 180 °C. IR (Nujol, KBr windows): ṽ = 3086 (w), 1568 (w), 1435 (m), 1282 (w), 1125 1097, 1048 (m), 907 (s), 820 (w), 744 (s), 696 (s), 641 (m), 563 (m), 508 (w). MS (DE): *m*/*z* (%) = 797 (<1) [{Py-CH_2NPOPh_2}-Fe_2Cl_2]$^+$, 760 (<1) [{Py-CH_2NPOPh_2}Fe_2Cl]$^+$, 670 (1) [{Py-CH_2NPOPh_2}Fe]$^+$, 578 (<1) [{Py-CH_2NPOPh_2}Fe{$NPOPh_2$}]$^+$, 292 (56) [{Py-$CH_2N(H)PPh_2$}Fe_2Cl_2]$^+$, 200 (100) [$HNPPh_2$]$^+$, 107 ([Py-CH_2NH]$^+$, 100). $C_{80}H_{80}Cl_2Fe_4N_8O_3P_4$ (1619.72): calcd. C 59.32, H 4.98, N 6.92; found C 56.70, H . 5.36, N 6.89.

Physical Data of [{2-Py-CH_2-*N*-P(*O*)Ph_2}FeCl]$_2$ (3): IR (Nujol, KBr windows): ṽ = 1605 (s), 1568 (m), 1482 (m), 1438 (s), 1359 (m), 1285 (m), 1258 (w), 1216 (w), 1153 (m), 1127 (vs), 1059 (s), 1021 (m), 998 (m), 944 (s), 834 (m), 767 (m), 726 (vs), 701 (s), 650 (m), 626 (m), 576 (s), 536 (s). MS (DE): *m*/*z* (%) = 796 (<1) [{Py-CH_2NPOPh_2}Fe_2Cl_2]$^+$, 760 (34) [{Py-CH_2NPOPh_2}Fe_2Cl]$^+$, 670 (22) [{Py-CH_2NPOPh_2}Fe]$^+$, 363 (3) [{Py-CH_2NPOPh_2}Fe]$^+$, 306 (3) [Py-$CHNPOPh_2$]$^+$, 201 (100) [$OPPh_2$]$^+$, 107 (24) [Py-CH_2NH]$^+$, 44 (100). $C_{36}H_{32}Cl_2Fe_2N_4O_2P_2$ (797.21): calcd. C 54.10, H 4.29, N 7.01; found C 54.46, H . 4.30, N 6.84.

[{2-Py-CH_2-*N*(H)-P(*O*)Ph_2}FeCl$_2$] (5): A 1.6 M solution of *n*BuLi in hexane (1.7 mL, 1.12 mmol) was dropped into a cooled solution (–78 °C) of 0.34 g of **1** (1.15 mmol) in 10 mL of THF. At –78 °C this red solution was added to a suspension of 0.19 g of $FeCl_3$ in 10 mL of THF. Thereafter the reaction mixture was warmed to room temp. and stirred for 24 h. Then all volatile materials were removed in vacuo. The dried residue was dissolved in 20 mL of CH_2Cl_2 and solid materials removed by filtration. At room temp. 0.05 g of colorless needles of **5** (0.11 mmol, 9%) formed; m.p. 219 °C. IR (Nujol, KBr windows): ṽ = 3220 (s), 1604 (m), 1589 (w), 1571 (w), 1480 (m), 1439 (s), 1309 (m), 1203 (w), 1143 (s), 1129 (m), 1099 (m), 1083 (m), 1069 (m), 1023 (w br), 996 (w), 976 (w), 968 (w), 889 (w), 860 (m), 762 (m), 729 (s), 698 (m), 608 (m), 564 (m), 519 (s). MS (DE): *m*/*z* (%) = 398 (4) [{Py-$CH_2NHPOPh_2$}FeCl]$^+$, 362 (2) [{Py-$CH_2NHPOPh_2$}Fe]$^+$, 308 (4) [Py-$CH_2NHPOPh_2$]$^+$, 201 (48) [$OPPh_2$]$^+$, 107 ([Py-CH_2NH]$^+$, 100). $C_{18}H_{17}Cl_2FeN_2OP$ (435.07): calcd. C 49.62, H 3.94, N 6.44; found C 47.33, H . 4.15, N 6.68.

Ph_2Si(NH-CH_2-2-Py)$_2$ (6): A solution of 1.5 mL of 2-pyridylmethylamine (14.4 mmol, 1.56 g) in 10 mL of toluene was cooled to –78 °C. Thereafter 9 mL of a 1.6 M *n*BuLi solution in hexane (14.4 mmol) were added dropwise. The solution turned violet. This solution was added very slowly at –78 °C to a pre-cooled solution of 1.5 mL dichloro-diphenylsilane (7.2 mmol, 1.82 g) in 5 mL of toluene. (Attention: Addition of the dichlorodiphenylsilane solution to the violet lithium 2-pyridylmethylamide solution lowered the yield significantly). After complete addition, the reaction mixture was slowly warmed to room temp. The precipitate (mainly LiCl) was removed by filtration. All volatile materials were removed from the filtrate by distillation under reduced pressure. The remaining brown oil solidified slowly within several days; yield 86%; m.p. 87 °C. IR (Nujol, KBr windows): ṽ = 3390 (s), 3046 (m), 2926 (vs), 2676 (vw), 1968 (vw), 1908 (vw), 1591 (s), 1567 (m), 1467 (vs), 1427 (vs), 1397 (vs), 1343 (m), 1219 (m), 1185 (vw), 1119 (vs), 1079 (s), 1046 (m), 993 (m), 961 (w), 889 (w), 850 (vs), 786 (s), 758 (vs), 745 (vs), 726 (s), 701 (vs), 680 (w), 620 (vw), 594 (m), 535 (s), 500 (s), 464 (m). ^{1}H NMR (200 MHz, [D$_6$]benzene): δ = 4.20 (d, 4 H, CH_2), 6.53 (m, 2 H, Pyr2), 6.77 (d, 2 H, Pyr4), 6.93 (dt, 2 H, Pyr3), 7.03–7.15 (m, Ph), 7.67–7.76 (m, Ph), 8.37–8.41 (m, Pyr1) ppm. ^{13}C{^{1}H} NMR (50 MHz, [D$_6$]benzene): δ = 47.2 (CH_2), 120.9 (Pyr2), 121.1 (Pyr4), 128.0 (Ph), 129.5 (Ph), 135.0 (Pyr3), 135.6 (Ph), 136.9 (Ph), 149.1 (Pyr1), 162.3 (Pyr5) ppm. MS (EI): *m*/*z* (%) = 397 (5) [M$^+$], 319 (100) [M – C_6H_6]$^+$; 289 (100) [M – $C_6H_7N_2$]$^+$; 260 (23); 211 (289 – C_6H_6, 100); 182 (50) [M – 2 Pyridyl]$^+$; 167 (20); 135 (80); 107 (100); 93 (80); 80 ([C_5H_6N]$^+$, 90). $C_{24}H_{24}N_4Si$ (396.56): calcd. C 72.68, H 6.10, N 14.13; found C 71.53, H . 6.29, N 13.50.

[Cl_2Fe_3{Ph_2Si(*N*-CH_2-2-Py)$_2$}$_2$] (7): A 1.6 M solution of *n*BuLi in hexane (1.6 mL, 2.56 mmol) was dropped at –78 °C into a solution of 0.50 g of **6** (1.23 mmol) in 10 mL of THF. This violet solution was added to a suspension of 0.24 g of anhydrous $FeCl_2$ (1.88 mmol) in 10 mL of THF. This solution was warmed to room temp., filtered and the volume of the solution reduced to half of the original volume. Storage at room temp. leads to the formation of 0.39 g of dark brown rod-shaped crystals of **7** (0.38 mmol, 60%); m.p. 215 °C. IR (Nujol, KBr windows): ṽ = 3042 (m), 1602 (w), 1565 (w), 1427 (s), 1280 (w), 1150 (w), 1113 (s), 1083 (vs), 1048 (m), 802 (s), 762 (m), 738 (m), 701 (s), 608 (w), 540 (m), 504 (m). MS (DE): *m*/*z* (%) = 486 (4) [Ph_2Si{NCH_2Py}$_2$FeCl]$^+$, 448 (10) [Ph_2Si{NCH_2Py}$_2$FeCl]$^+$, 319 (25) [$PhSi${NCH_2Py}$_2$]$^+$, 289 (100) [Ph_2Si{NCH_2Py}]$^+$, 198 (35) [ClFeNHCH_2Py]$^+$, 181 (15) [$SiPh_2$]$^+$, 137 (15) [Py-CH_2 – $NHSiH_2$]$^+$, 108 (100) [Py-CH_2–NH_2]$^+$, 79 ([Py]$^+$, 85). $C_{48}H_{44}Cl_2Fe_3N_8Si_2$ (1027.52): calcd. C 56.10, H 4.32, N 10.91; found C 55.42, H . 4.58, N 10.43.

X-ray Structure Determinations: The intensity data for the compounds were collected on a Nonius KappaCCD diffractometer using graphite-monochromated Mo-K_α radiation. Data was corrected for Lorentz and polarization effects but not for absorption effects.[43,44] The structures were solved by direct methods (SHELXS[45]) and refined by full-matrix least-squares techniques against F_o^2 (SHELXL-97[45]). The hydrogen atoms for the amine groups compound **5** and **6** were located by difference Fourier synthesis and refined isotropically.[45] All other hydrogen atoms were included at calculated positions with fixed thermal parameters. All non-hydrogen atoms were refined anisotropically.[45] Crystallographic data as well as structure solution and refinement details are summarized in Table 1. XP (SIEMENS Analytical X-ray Instruments, Inc.) was used for structure representations.

CCDC-798041 (for **2**), -798042 (for **4**), -798043 (for **5**), -798044 (for **6**), and -798045 (for **7**). Copies of the data can be obtained free of charge on application to CCDC, 12 Union Road, Cambridge CB2 1EZ, UK [E-mail: deposit@ccdc.cam.ac.uk]. Supplementary material regarding the magnetic properties is also available.

Supporting Information (see footnote on the first page of this article): Derivation of the equation for the magnetic susceptibility.

Acknowledgments

We thank the Deutsche Forschungsgemeinschaft (DFG) for generous financial support. A. M. is thankful to the Carl-Zeiss-Stiftung

(Stuttgart, Germany) for a Ph. D. stipend. The authors also acknowledge the help of Mrs. C. Felbel and Prof. Dr. W. Plass.

[1] a) D. M. Roundhill, *Chem. Rev.* **1992**, *92*, 1–27; b) W. Kaim, B. Schwederski: *Bioinorganic Chemistry: Inorganic Elements in the Chemistry of Life*, Wiley: Chichester, **1994**; c) R. H. Holm, P. Kennepohl, E. I. Solomon, *Chem. Rev.* **1996**, *96*, 2239–2314; d) J. J. R. Fraústo da Silva, R. J. P. Williams: *The Biological Chemistry of the Elements*, 2nd ed., Oxford University Press, Oxford, **2001**; e) T. A. Jackson, L. Que, in: *Concepts and Models in Bioinorganic Chemistry* (Eds.: H.-B. Kraatz, N. Metzler-Nolte), Wiley-VCH, Weinheim, **2006**, p. 259–286.

[2] a) Y. Okamoto, K. Ogura, T. Kinoshita, *Polyhedron* **1984**, *3*, 635–638; b) K. Ogura, Y. Kurasawa, Y. Yamaguchi, Y. Okamoto, *Heterocycles* **2003**, *59*, 283–291.

[3] K. Chen, M. Costas, L. Que, *J. Chem. Soc., Dalton Trans.* **2002**, 672–679.

[4] A. L. Gavrilova, B. Bosnich, *Chem. Rev.* **2004**, *104*, 349–383.

[5] M. Costas, M. P. Mehn, M. P. Jensen, L. Que, *Chem. Rev.* **2004**, *104*, 939–986.

[6] X. Shan, L. Que, *J. Inorg. Biochem.* **2006**, *100*, 421–433.

[7] M. Ostermeier, C. Limberg, B. Ziemer, V. Karunakaran, *Angew. Chem.* **2007**, *119*, 5423–5426; *Angew. Chem. Int. Ed.* **2007**, *46*, 5329–5331.

[8] K. Visvaganesan, R. Mayilmurugan, E. Suresh, M. Palaniandavar, *Inorg. Chem.* **2007**, *46*, 10294–10306.

[9] M. Westerhausen, T. Bollwein, N. Makropoulos, S. Schneiderbauer, M. Suter, H. Nöth, P. Mayer, H. Piotrowski, K. Polborn, A. Pfitzner, *Eur. J. Inorg. Chem.* **2002**, 389–404.

[10] M. Westerhausen, A. N. Kneifel, N. Makropoulos, *Inorg. Chem. Commun.* **2004**, *7*, 990–993.

[11] M. Westerhausen, A. N. Kneifel, P. Mayer, *Z. Anorg. Allg. Chem.* **2006**, *632*, 634–638.

[12] a) J. T. B. H. Jastrzebski, J. M. Klerks, G. van Koten, K. Vrieze, *J. Organomet. Chem.* **1981**, *210*, C49–C53; b) G. van Koten, J. T. B. H. Jastrzebski, K. Vrieze, *J. Organomet. Chem.* **1983**, *250*, 49–61; c) E. Wissing, S. van der Linden, E. Rijnberg, J. Boersma, W. J. J. Smeets, A. L. Spek, G. van Koten, *Organometallics* **1994**, *13*, 2602–2608.

[13] M. Westerhausen, T. Bollwein, N. Makropoulos, T. M. Rotter, T. Habereder, M. Suter, H. Nöth, *Eur. J. Inorg. Chem.* **2001**, 851–857.

[14] M. Westerhausen, T. Bollwein, P. Mayer, H. Piotrowski, A. Pfitzner, *Z. Anorg. Allg. Chem.* **2002**, *628*, 1425–1432.

[15] C. C. Lu, E. Bill, T. Weyhermüller, E. Bothe, K. Wieghardt, *J. Am. Chem. Soc.* **2008**, *130*, 3181–3197.

[16] a) G. Chen, Y.-X. Sun, M. Sun, W. Qi, *Acta Crystallogr., Sect. E* **2004**, *60*, m1547–m1549; b) K. W. Törnroos, D. Chernyshov, M. Hostettler, H.-B. Bürgi, *Acta Crystallogr., Sect. C* **2005**, *61*, m450–m452.

[17] A. Malassa, H. Görls, A. Buchholz, W. Plass, M. Westerhausen, *Z. Anorg. Allg. Chem.* **2006**, *632*, 2355–2362.

[18] a) D. C. Bradley, M. H. Chisholm, *Acc. Chem. Res.* **1976**, *9*, 273–280; b) M. F. Lappert, P. P. Power, A. R. Sanger, R. C. Srivastava, *Metal and Metalloid Amides: Syntheses, Structures, and Physical and Chemical Properties*, Ellis Horwood, Chichester, **1980**, chapter 8, p. 465–544; c) M. Lappert, A. Protchenko, P. Power, A. Seeber, *Metal Amide Chemistry*, Wiley, Chichester, **2009**, chapter 6, p. 149–204.

[19] N. Y. M. Iha, M. A. de Almeida Azzelini, S. Utsuno, *Polyhedron* **1998**, *17*, 3379–3390.

[20] A. Malassa, N. Herzer, H. Görls, M. Westerhausen, *Dalton Trans.* **2010**, *39*, 5356–5366.

[21] V. G. Gibson, R. K. O'Reilly, D. F. Wass, A. J. P. White, D. J. Williams, *Dalton Trans.* **2003**, 2824–2830.

[22] C. J. Davies, G. A. Solan, J. Fawcett, *Polyhedron* **2004**, *23*, 3105–3114.

[23] A. Malassa, C. Agthe, H. Görls, M. Friedrich, M. Westerhausen, *J. Organomet.-Chem.* **2010**, *695*, 1641–1650.

[24] B. A. Frazier, P. T. Wolczanski, E. B. Lobkovsky, T. R. Cundari, *J. Am. Chem. Soc.* **2009**, *131*, 3428–3429.

[25] M. Westerhausen, A. N. Kneifel, *Inorg. Chem. Commun.* **2004**, *7*, 763–766.

[26] C. Tejel, M. A. Ciriano, M. P. del Río, F. J. van den Bruele, D. G. H. Hetterscheid, N. T. i Spithas, B. de Bruin, *J. Am. Chem. Soc.* **2008**, *130*, 5844–5845.

[27] a) S. Thewissen, M. D. M. Reijnders, J. M. M. Smits, B. de Bruin, *Organometallics* **2005**, *24*, 5964–5972; b) C. Tejel, M. A. Ciriano, M. P. del Río, D. G. H. Hetterscheid, N. T. i Spithas, J. M. M. Smits, B. de Bruin, *Chem. Eur. J.* **2008**, *14*, 10932–10936; c) C. Tejel, M. P. del Río, M. A. Ciriano, E. J. Reijerse, F. Hartl, S. Záliš, D. G. H. Hetterscheid, N. T. i Spithas, B. de Bruin, *Chem. Eur. J.* **2009**, *15*, 11878–11889.

[28] D. Olbert, A. Kalisch, H. Görls, I. M. Ondik, M. Reiher, M. Westerhausen, *Z. Anorg. Allg. Chem.* **2009**, *635*, 462–470.

[29] M. M. Olmstead, P. P. Power, S. C. Shoner, *Inorg. Chem.* **1991**, *30*, 2547–2551.

[30] F. A. Cotton, L. M. Daniels, L. R. Falvello, J. H. Matonic, C. A. Murillo, X. Wang, H. Zhou, *Inorg. Chim. Acta* **1997**, *266*, 91–102.

[31] F. A. Cotton, L. M. Daniels, G. T. Jordan, C. A. Murillo, I. Pascual, *Inorg. Chim. Acta* **2000**, *297*, 6–10.

[32] A. Maercker, *Angew. Chem.* **1987**, *99*, 1002–1019; *Angew. Chem. Int. Ed. Engl.* **1987**, *26*, 972–989.

[33] a) R. E. Mulvey, V. L. Blair, W. Clegg, A. R. Kennedy, J. Klett, L. Russo, *Nat. Chem.* **2010**, *2*, 588–591; b) S. Krieck, H. Görls, M. Westerhausen, *J. Organomet. Chem.* **2009**, *694*, 2204–2209; c) J. Langer, S. Krieck, R. Fischer, H. Görls, D. Walther, M. Westerhausen, *Organometallics* **2009**, *28*, 5814–5820; d) A. R. Kennedy, J. Klett, R. E. Mulvey, D. S. Wright, *Science* **2009**, *326*, 706–708; e) M. Gärtner, H. Görls, M. Westerhausen, *J. Organomet. Chem.* **2008**, *693*, 221–227; f) M. Gärtner, H. Görls, M. Westerhausen, *Synthesis* **2007**, 725–730.

[34] X. Guo, S. Pan, J. Liu, Z. Li, *J. Org. Chem.* **2009**, *74*, 8848–8851.

[35] E. Bartmann, *J. Organomet. Chem.* **1985**, *284*, 149–158.

[36] J. Zeller, S. König, U. Radius, *Inorg. Chim. Acta* **2004**, *357*, 1813–1821.

[37] M. T. Hay, B. J. Hainaut, S. J. Geib, *Inorg. Chem. Commun.* **2003**, *6*, 431–434.

[38] R. Vollmerhaus, R. Tomaszewski, P. Shao, N. J. Taylor, K. J. Wiacek, S. P. Lewis, A. Al-Humydi, S. Collins, *Organometallics* **2005**, *24*, 494–507.

[39] M. Podewitz, C. Herrmann, A. Malassa, M. Westerhausen, M. Reiher, *Chem. Phys. Lett.* **2008**, *451*, 301–308.

[40] O. Kahn, *Molecular Magnetism*, VCH, Weinheim, Germany, **1993**.

[41] J. S. Duncan, T. M. Nazif, A. K. Verma, S. C. Lee, *Inorg. Chem.* **2003**, *42*, 1211–1224.

[42] D. Olbert, H. Görls, D. Conrad, M. Westerhausen, *Eur. J. Inorg. Chem.* **2010**, 1791–1797.

[43] *COLLECT*, Data Collection Software, Nonius B. V., The Netherlands, **1998**.

[44] *Processing of X-ray Diffraction Data Collected in Oscillation Mode*: Z. Otwinowski, W. Minor, in: *Methods in Enzymology* (Eds.: C. W. Carter, R. M. Sweet), vol. 276, *Macromolecular Crystallography*, part A, p. 307–326, Academic Press, **1997**.

[45] G. M. Sheldrick, *Acta Crystallogr., Sect. A* **2008**, *64*, 112–122.

Received: November 3, 2010
Published Online: February 15, 2011

